Mechanistic and Structural Analysis of Aminoglycoside *N*-Acetyltransferase AAC(6′)-Ib and Its Bifunctional, Fluoroquinolone-Active AAC(6′)-Ib-cr Variant[†,‡]

Matthew W. Vetting,[§,||] Chi Hye Park,[§,⊥] Subray S. Hegde,[§,||] George A. Jacoby,[#] David C. Hooper,[⊥] and John S. Blanchard*[,||]

Department of Biochemistry, Albert Einstein College of Medicine, 1300 Morris Park Avenue, Bronx, New York 10461, Harvard Medical School, Division of Infectious Diseases, Massachusetts General Hospital, 55 Fruit Street, GRJ 512, Boston, Massachusetts 02114, and Lahey Clinic, 41 Mall Road, Burlington, Massachusetts 01805

Received April 15, 2008; Revised Manuscript Received July 15, 2008

ABSTRACT: Enzymatic modification of aminoglycoside antibiotics mediated by regioselective aminoglycoside *N*-acetyltransferases is the predominant cause of bacterial resistance to aminoglycosides. A recently discovered bifunctional aminoglycoside acetyltransferase (AAC(6′)-Ib variant, AAC(6′)-Ib-cr) has been shown to catalyze the acetylation of fluoroquinolones as well as aminoglycosides. We have expressed and purified AAC(6′)-Ib-wt and its bifunctional variant AAC(6′)-Ib-cr in *Escherichia coli* and characterized their kinetic and chemical mechanism. Initial velocity and dead-end inhibition studies support an ordered sequential mechanism for the enzyme(s). The three-dimensional structure of AAC(6′)-Ib-wt was determined in various complexes with donor and acceptor ligands to resolutions greater than 2.2 Å. Observation of the direct, and optimally positioned, interaction between the 6′-NH_2 and Asp115 suggests that Asp115 acts as a general base to accept a proton in the reaction. The structure of AAC(6′)-Ib-wt permits the construction of a molecular model of the interactions of fluoroquinolones with the AAC(6′)-Ib-cr variant. The model suggests that a major contribution to the fluoroquinolone acetylation activity comes from the Asp179Tyr mutation, where Tyr179 makes π-stacking interactions with the quinolone ring facilitating quinolone binding. The model also suggests that fluoroquinolones and aminoglycosides have different binding modes. On the basis of kinetic properties, the pH dependence of the kinetic parameters, and structural information, we propose an acid/base-assisted reaction catalyzed by AAC(6′)-Ib-wt and the AAC(6′)-Ib-cr variant involving a ternary complex.

Aminoglycosides and fluoroquinolones are broad spectrum bactericidal antimicrobial agents that are widely used in the treatment of variety of Gram-positive and Gram-negative bacterial infections. They are chemically and structurally distinct compounds that inhibit different but essential cellular functions of bacteria. Aminoglycosides inhibit bacterial protein synthesis by binding to the A site of 16S rRNA causing misreading and/or hindering of the translocation step, while fluoroquinolones exert their antibacterial activity by interacting with DNA gyrase and DNA topoisomerase IV. With the increased usage of these antimicrobials, bacteria have developed a variety of resistance mechanisms to evade their deadly effects. Enzymatic modification of aminoglycosides, namely, *O*-phosphorylation, *O*-nucleotidylation, and *N*-acetylation catalyzed by aminoglycoside phosphotransferases (APHs), aminoglycoside nucleotidyltransferases (ANTs), and aminoglycoside acetyltransferases (AACs),[1] respectively, is the predominant cause of bacterial resistance to aminoglycosides (*1*−*4*), whereas drug efflux and target gene mutations are major causes of fluoroquinolone resistance (*5*−*8*). Recently, plasmid borne, horizontally transferable, Qnr-mediated target protection has emerged as a new fluoroquinolone resistance mechanism among Gram-negative pathogens worldwide (*9*−*12*).

Among aminoglycoside-modifying enzymes, each class is divided into subtypes based on the regioselectivity of substrate modification. Aminoglycoside *N*-acetyltransferases selectively transfer an acetyl group from acetyl-CoA (AcCoA) to one of the several amine functions present in aminoglycosides. There are four major classes of AACs: AAC(1), AAC(3), AAC(2′), and AAC(6′), designated according to the site of acetylation (*1*). AAC(6′) family members are most common in nature and of particular importance since they modify aminoglycosides most used

[†] This work was supported by NIH Grants A160899 (to J.S.B.), T32 AI07501 (to M.W.V.), AI057576 (to D.C.H.), and AI043312 (to G.A.J.).

[‡] Atomic coordinates and structure factors (codes 1v0c, 2bue, and 2vqy) have been deposited in the Protein Data Bank, Research Collaboratory for Structural Bioinformatics, Rutgers University, Rutgers, NJ (http://www.rcsb.org).

* Corresponding author. Phone: (718) 430-3096. Fax: (718) 430-3096. E-mail: blanchar@aecom.yu.edu.

[§] These authors have contributed equally.

[||] Albert Einstein College of Medicine.

[⊥] Harvard Medical School.

[#] Lahey Clinic.

[1] Abbreviations: AcCoA, acetyl-coenzyme A; AAC, aminoglycoside *N*-acetyltransferase; DTP, 4,4′-dithiopyridine; DTNB, 5,5′-dithiobis(2-nitrobenzoic acid); GNATs, GCN5-related *N*-acetyltransferases; HEPES, 4-(2-hydroxylethyl)-1-piperazineethanesulfonic acid; IPTG, isopropyl thio-β-D-galactosidase; KAN, kanamycin; MES, 2-(*N*-morpolino)ethanesulfonic acid; PAR, paromomycin; RIB, ribostamycin; rmsd, root-mean-square deviation; SDS−PAGE, sodium dodecyl sulfate−polyacrylamide gel electrophoresis; TAPS, *N*-tris(hydroxymethyl)methyl-3-aminopropanesulfonic acid.

10.1021/bi800664x CCC: $40.75
Published on Web 08/19/2008

in chemotherapy (*1, 13*). The AAC(6′) class is further divided into two subtypes of which the AAC(6′)-I subtype is most prevalent (*1, 14*). Aminoglycoside-modifying enzymes are generally monofunctional with the exception of a few bifunctional enzymes such as AAC(6′)/APH(2″), ANT(3″)-Ii/AAC(6′)-IId, and AAC(3)-Ib/AAC(6′)-Ib′ (*15*−*20*), all of which modify aminoglycosides.

AAC(6′)-Ib, the most prevalent aminoglycoside modifying enzyme (*13*) that confers resistance to tobramycin, kanamycin, and amikacin, was first identified in *Klebsiella pneumoniae* isolates in 1986 (*21*). Since then several variants of this enzyme have been described (*13, 22*). Recently, we identified an AAC(6′)-Ib variant designated as AAC(6′)-Ib-cr, which contains two unique amino acid substitutions, namely, Trp102Arg and Asp179Tyr, which are not found in other variants. AAC(6′)-Ib-cr, unlike other AAC(6′)-Ib variants and bifunctional aminoglycoside-modifying enzymes, in addition to acetylating aminoglycosides, also acetylates ciprofloxacin and norfloxacin belonging to an entirely different class of antibacterials and thus provides low-level resistance against these fluoroquinolones (*22*). In this paper we describe the kinetic characterization of AAC(6′)-Ib-cr and its wild-type parent enzyme along with the three-dimensional structure of the wild-type enzyme.

MATERIALS AND METHODS

Materials. All chemicals, reagents, acetyl-coenzyme A, and aminoglycosides were purchased from Sigma-Aldrich Chemical Co. Enzymes used in molecular biology were supplied by New England Biolabs. Plasmid pET-28a and *Escherichia coli* strains Nova Blue and BL21(DE3) were obtained from Novagen.

Cloning, Overexpression, and Purification of AAC(6′)-Ib-wt and AAC(6′)-Ib-cr. The open reading frames of *aac(6′)-Ib-wt* (where −*wt* stands for wild type) and *aac(6′)-Ib-cr* were amplified by standard PCR techniques using as template transconjugant *E. coli* J53 pHSH10-2 (*22*). Oligonucleotides AC6F (5′- ATCCCGCTCATATGAGTATTCAACATTTC-3′) and AC6R (5′-ATCCCGCTAAGCTTTCACTCCTCT-GTTGCCAT-3′) containing the underlined *Nde*I and *Hin*dIII restriction sites, respectively, were used for *aac(6′)-Ib*, while AC6crF(5′-ATCCCGCTGCTAGCAACGCAAAAACAAAG-3′) and A6CcrR (5′-ATCCCGCTAAGCTTTTAGGCAT-CACTGCGTGTTCG-3′) containing the underlined *Nhe*I and *Hin*dIII restriction sites, respectively, were used for *aac(6′)-Ib-cr*. The PCR fragments were cloned into pET-28a(+), and the recombinant AAC(6′)-Ib-wt and AAC(6′)-Ib-cr bearing a thrombin-cleavable N-terminal His_6 tag were expressed in *E. coli* strain BL21(DE3). For shake flask growth, 1 L of Luria broth medium supplemented with kanamycin (35 μg/mL) was inoculated with 10 mL of an overnight culture and incubated at 37 °C. The culture was grown to midlog phase ($A_{600} \sim 0.8$), cooled to 20 °C, induced with 0.5 mM IPTG, and further incubated overnight at 20 °C.

All purification procedures were carried out at 4 °C. The cells were collected by centrifugation at 1200*g* and resuspended in buffer A (50 mM Tris, pH 7.8, containing 150 mM NaCl) containing protease inhibitors, lysozyme (5 μg/mL), and DNase I (0.1 μg/mL) and stirred for 20 min. The cells were then lysed by sonication, and cell debris was removed by centrifugation at 10000*g* for 30 min. The supernatant was dialyzed against buffer A, loaded onto a Ni-NTA column preequilibrated with buffer A, and washed with 10 column volumes of the same buffer. The bound proteins were eluted with a linear 0−0.3 M imidazole gradient at a flow rate of 1 mL/min. The active fractions were pooled and concentrated to 5 mL by ultrafiltration. The His_6 tag was then cleaved using thrombin (2 units/mg of protein), and the solution was dialyzed overnight against buffer A containing 2 mM $CaCl_2$ and loaded onto a Superdex S-75 column preequilibrated with buffer A. Pure fractions as determined by SDS−PAGE were pooled and concentrated by ultrafiltration. Protein concentrations were estimated by the Bio-Rad protein assay method using bovine serum albumin as a standard.

Measurement of Enzyme Activity. Reaction rates were measured spectrophotometrically by following the increase in absorbance at 324 or 412 nm due to the reaction between the free sulfhydryl group of CoASH, generated by the enzyme-catalyzed aminoglycoside/fluoroquinolone acetylating activity, and 4,4′-dithiopyridine (DTP) or 5,5′-dithiobis(2-nitrobenzoic acid) (DTNB). The reaction was monitored continuously on a UVIKON XL spectrophotometer, and enzyme activities were calculated using a molar absorption coefficient of either 19800 M^{-1} cm^{-1} (DTP) or 13600 M^{-1} cm^{-1} (DTNB). Assay mixtures contained appropriate buffer, 0.05 mM DTP or 0.1 mM DTNB, in addition to substrates or inhibitors in a volume of 1 mL. Reactions were initiated by the addition of enzyme and followed at room temperature for 1−2 min.

Initial Velocity Experiments. Initial velocity kinetic data were fitted using Sigma Plot 2000. Kinetic constants for aminoglycosides and ciprofloxacin were determined using fixed, saturating conditions of AcCoA. Kinetic constants for AcCoA were determined at fixed, saturating concentrations of kanamycin and ciprofloxacin. Individual substrate saturation kinetic data were fitted to eq 1

$$v = VA/(A + K) \quad (1)$$

where V is the maximal velocity, A is the substrate concentration, and K is the Michaelis−Menten constant (K_m). Initial velocity patterns were obtained by measuring the initial rate at five concentrations of each substrate. Equation 2 was used to fit the intersecting initial velocity pattern:

$$v = VAB/(K_{ia}K_B + K_aB + K_BA + AB) \quad (2)$$

where A and B are the concentrations of the substrates, K_a and K_B are the Michaelis−Menten constants for the substrates, and K_{ia} is the inhibition constant for substrate A.

Dead-End Inhibition Patterns. Dead-end inhibition patterns were determined by measuring initial velocities at variable concentrations of one reactant, the second reactant concentration fixed, and the dead-end inhibitors (lividomycin and pefloxacin) at several concentrations. Equations 3 and 4 were used to fit the competitive and uncompetitive inhibition, respectively.

$$v = VA/[K_a(1 + I/K_{is}) + A] \quad (3)$$

$$v = VA/[K_a + A(1 + I/K_{ii})] \quad (4)$$

where I is the inhibitor concentration and K_{is} and K_{ii} are the slope and intercept inhibition constants for the inhibitor, respectively.

Dependence of Acetylation Activity on pH. The pH dependence of the kinetic parameters exhibited by AAC(6′)-Ib-wt and AAC(6′)-Ib-cr was determined at the saturating concentrations of substrates. Activities were monitored every 0.3 pH unit from pH 4.4 to pH 6.7 for AAC(6′)-Ib, from pH 5.2 to pH 7.3 for AAC(6′)-Ib-cr for aminoglycoside substrates, and from pH 6.7 to pH 9.1 for fluoroquinolone acetylation using the following buffers: citrate−phosphate (pH 4.4−6.2), MES (pH 5.2−6.6), HEPES (pH 6.7−7.9), and TAPS (pH 7.6−9.1). Profiles were generated by plotting the log of k_{cat} versus the pH and fitted using the equations:

$$\log k_{cat} = \log\left[C/\left(1 + H^+/K_a + K_b/H^+\right)\right] \quad (5)$$

where C is the pH-independent plateau value, K_a is the ionization constant for the acidic group, K_b is the ionization constant for the basic group, and H^+ is the hydrogen ion concentration.

Solvent Kinetic Isotope Effects. The solvent kinetic isotope effects on k_{cat} and k_{cat}/K_m were determined by measuring the initial velocities using saturating concentrations of AcCoA while varying the concentrations of either kanamycin B at pH 6.1 or ciprofloxacin at pH 7.8 in either H_2O or 95% D_2O. Solvent deuterium kinetic isotope effects were fitted to the equation:

$$v = VA/[KA(1 + F_iE_{V/K}) + A(1 + F_iE_V)] \quad (6)$$

where $E_{V/K}$ and E_V are the isotope effects on $k_{cat}/K_m - 1$ and $k_{cat} - 1$, respectively, and F_i represents the fraction of isotope.

Crystallization and Data Collection. AAC(6′)-Ib-wt was crystallized by vapor diffusion under oil. Several commercial crystallization screens were used, resulting in only two crystallization hits, both containing calcium acetate. Optimization of conditions yielded a crystallization solution of 20% PEG 3350, 200 mM calcium acetate, and 100 mM sodium cacodylate, pH 6.75. The protein solution (3 μL of a 10 mg/mL, 20 mM Tris, pH 7.5, 20 mM NaCl, 3 mM AcCoA) was combined with 3 μL of the crystallization solution under 150 μL of FISHER brand silicone oil in 96-well round-bottom plates stored open to room humidity. The crystals grew to maximum dimensions of 0.1 × 0.1 × 0.25 mm within 7 days, exhibiting bipyramidal morphology. Crystals were soaked for 10 s in 20% PEG 6000, 200 mM calcium acetate, 100 mM sodium cacodylate, pH 6.75, and 20% glycerol prior to vitrification by immersion in liquid nitrogen. All data were collected at 100 K using an R-Axis IV++ image plate detector using Cu Kα radiation from a Rigaku RU-H3R X-ray generator and processed using MOSFLM (*23*) and SCALA (*24*). The crystals belong to space group $P4_32_12$ with approximate unit cell dimensions of $a = b = 57.3$ Å and $c = 148.4$ Å. There is one molecule per asymmetric unit with a solvent content of 55.4%.

Phasing and Structure Refinement. The structure of AAC(6′)-Ib-wt was determined by SAD (single-wavelength anomalous diffraction). A single crystal was soaked for 20 min in an 8 mM mercury acetate doped solution (20% PEG 6000, 200 mM calcium acetate, and 100 mM sodium cacodylate, pH 6.75) and subsequently swept through the cryoprotectant solution (see above) prior to vitrification by immersion in liquid nitrogen. Heavy atom positions and initial phases were determined using PHENIX (*25*). The majority of the structure was fit to the solvent-flattened SAD map utilizing the autobuilding program ARP/WARP (*26*). The remainder of the structure was fit manually using iterative rounds of modeling building within the molecular graphics program COOT (*27*) followed by refinement against the data using REFMAC (*28*). Stereochemical parameters for the ligands were calculated using the PRODRG (*29*) server. The ligands were not added until the final rounds of refinement to minimize model bias.

Table 1: Kinetic Parameters for Acetyl-CoA, Aminoglycosides, and Fluoroquinolones

substrate	K_m (μM)	k_{cat} (min^{-1})	V/K (M^{-1} min^{-1} × 10^6)
AAC(6′)-Ib-wt			
kanamycin B[a]	0.27 ± 0.01	136 ± 3	503
neomycin B[a]	20 ± 1	185 ± 3	9
acetyl-CoA[b]	35 ± 2	139 ± 4	4
ciprofloxacin	NA[d]		
AAC(6′)-Ib-cr			
kanamycin B[a]	6.7 ± 0.4	315 ± 5	47
neomycin B[a]	ND[e]		
acetyl-CoA [b]	5.3 ± 0.2	314 ± 3	59
ciprofloxacin[a]	70 ± 6	62 ± 2	0.9
norfloxacin[a]	67 ± 6	65 ± 4	
acetyl-CoA [c]	108 ± 10	62 ± 2	0.6

[a] Measured at fixed saturating concentration of AcCoA. [b] Measured at fixed saturating concentration of kanamycin B. [c] Measured at fixed saturating concentration of ciprofloxacin. [d] NA = no activity. [e] ND = not determined.

Aminoglycoside Complexes. Single crystals were soaked in 100 mM sodium cacodylate, pH 6.5, 20% PEG 6000, 200 mM calcium acetate, and either 5 mM RIB or 10 mM PAR for either 1 h (RIB) or 2 h (PAR). Crystals were then streaked through an identical solution that included 20% glycerol and vitrified by immersion in liquid nitrogen.

Ciprofloxacin Model. Manual manipulation of the conformation and docking of ciprofloxacin to AAC(6′)-Ib was performed using the molecular graphics program COOT (*27*) with stereochemical restraints calculated using the PRODRG (*29*) server.

RESULTS AND DISCUSSION

Substrate Specificities of AAC(6′)-Ib-wt and AAC(6′)-Ib-cr. Initial velocities were determined at the optimum pH (see below) at 8−10 different concentrations of each substrate. The data were plotted by nonlinear, least-squares curve fitting using Sigmaplot (version 2000). Kinetic constants for AcCoA, determined at saturating concentrations of kanamycin B and ciprofloxacin, are presented in Table 1. The steady-state kinetic parameters for aminoglycosides and fluoroquinolones at saturating concentrations of AcCoA are also summarized in Table 1.

From the determined steady-state kinetic parameters, particularly the relative V/K values, AcCoA was the strongly preferred acyl donor while other coenzyme A derivatives were either extremely poor substrates or did not demonstrate any activity (data not shown). AAC(6′)-Ib-wt exhibited somewhat broader specificity with respect to aminoglycosides when compared to AAC(6′)-Ib-cr. Among 4,6-disubstituted aminoglycosides (Figure S1), kanamycin B was the best substrate (Table 1) while tobramycin and kanamycin A exhibited very similar values. Among 4,5-disubstituted aminoglycosides, neomycin B exhibited significant activity, while ribostamycin was a poor substrate (data not shown).

Another 4,5-disubstituted aminoglycoside, lividomycin A that contains a 6′-hydroxyl group, was a good inhibitor of AAC(6′)-Ib and was used in dead-end inhibition studies. Substrate specificities for AAC(6′)-Ib-cr were somewhat different. Similar to AAC(6′)-Ib-wt, AcCoA was the strongly preferred acyl donor. Surprisingly, the *V*/*K* value of AcCoA increased 15-fold for AAC(6′)-Ib-cr due to both increases in k_{cat} and a decreased K_m value (Table 1). The V/K_{AcCoA} for fluoroquinolone acetylation, however, was about 100-fold lower compared to aminoglycoside acetylation. Substrate specificity for kanamycin decreased by a modest 10-fold when compared to wild type, while neomycin B exhibited extremely low activity that could not be measured with certainty. Among the fluoroquinolones tested, ciprofloxacin and norfloxacin exhibited acetylating activity (Table 1) while tosulfloxacin exhibited very low but measurable activity (data not shown). Fluoroquinolones that contain one or more substituents on the carbon atoms adjacent to piperazinyl nitrogen (gatifloxacin and sparfloxacin) were not acetylated by AAC(6′)-Ib-cr while pefloxacin, which contains a substituted piperazinyl nitrogen, was an inhibitor of AAC(6′)-Ib-cr. The catalytic efficiency of fluoroquinolone acetylation was about 50 times lower compared to kanamycin.

Kinetic Mechanism. The initial velocity pattern for AAC(6′)-Ib-cr was determined using both ciprofloxacin and AcCoA (Figure 1) and kanamycin and AcCoA (data not shown). The resultant double-reciprocal plots were intersecting. The intersecting initial velocity plots suggest a sequential kinetic mechanism, where both substrates must be bound to the enzyme for catalysis to occur. A sequential kinetic mechanism could proceed through either ordered or random addition of substrates. Dead-end inhibitors are powerful tools in determining the order of substrate additions. Dead-end inhibition studies were carried out using both fluoroquinolone (pefloxacin) and aminoglycoside (lividomycin A) inhibitors (Figure 1, Table 2). Lividomycin A displayed linear competitive inhibition versus both kanamycin and ciprofloxacin and uncompetitive inhibition versus AcCoA (Figure 1). Similarly, pefloxacin exhibited linear competitive inhibition versus both kanamycin and norfloxacin and uncompetitive inhibition versus AcCoA (Table 2). These data are consistent with the ordered addition of AcCoA followed by aminoglycoside or fluoroquinolone. In addition, Kim et al. have recently reported an ordered sequential kinetic mechanism (where AcCoA binds first) for an AAC(6′)-Ib variant, namely, AAC(6′)-Ib′ from a bifunctional AAC(3)-Ib/AAC(6′)-Ib′ based on their dead-end and product inhibition studies (*15*). AAC(6′)-Ib-wt has an additional 15 residues at the N-terminus compared to the AAC(6′)-Ib′ variant described by Kim et al. (*15*). AAC(6′)-Ib-wt also has two conservative amino acid substitutions, L2V and V26L, compared to AAC(6′)-Ib′. AAC(6′)-Ib-wt and AAC(6′)-Ib′ exhibit similar kinetic properties on overlapping substrates tested for both enzymes. However, the pH ranges of their optimal activities differ significantly. The optimum pH for aminoglycoside acetylation by AAC(6′)-Ib-wt is 5.6 while AAC(6′)-Ib′ has an optimal pH of around 7.5 (*15*) where AAC(6′)-Ib-wt exhibits less than 5% of its maximal activity. Well over 50 unique AACs have been identified among bacteria (*1, 13*), and several AACs have been subjected to the analysis of their kinetic mechanisms (*15, 19, 30*−*35*). The majority of the AACs studied to date use a random sequential mechanism

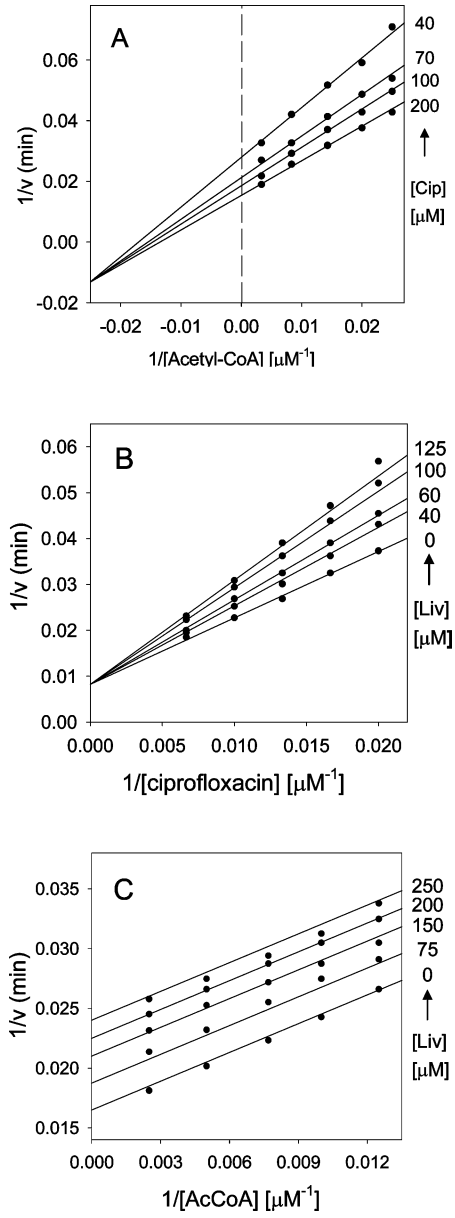

FIGURE 1: Initial velocity pattern and dead-end inhibition of AAC(6′)-Ib-cr. (A) Initial velocity pattern. The symbols are experimentally determined values, while the lines are fits of the data to eq 2. (B) Inhibition pattern of lividomycin A versus ciprofloxacin at a fixed saturating concentration of AcCoA. (C) Inhibition pattern of lividomycin A versus AcCoA at a fixed saturating fixed saturating concentration of ciprofloxacin. Symbols are experimentally determined values while the lines are fits of the data to eqs 3 and 4, respectively.

while a few others, including AAC(6′)-Ib, use an ordered sequential mechanism (*15, 19, 35*).

Studies of solvent kinetic isotope effects can be a useful tool in the determination of rate-limiting nature of the chemical reaction and the kinetic mechanism, especially to distinguish between steady-state and rapid equilibrium mechanisms. In a rapid equilibrium kinetic mechanism, the rates of substrate binding and product dissociation are very fast relative to the catalytic step, and equivalent isotope effects must be observed on *V* and *V*/*K*. This is not a requirement for the steady-state mechanism. Solvent kinetic isotope effects for kanamycin B and ciprofloxacin acetylation were determined at pH 6.0 and 7.7, respectively, in both H_2O and

Table 2: Dead-End Inhibition Patterns for AAC(6′)-Ib-cr

inhibitor	variable substrate	fixed substrate (μM)	pattern	K_i (μM)	K_{ii} (μM)
lividomycin A	ciprofloxacin	AcCoA (400)	C	220 ± 10	
lividomycin A	kanamycin B	AcCoA (200)	C	19 ± 1	
lividomycin A	AcCoA	ciprofloxacin (200)	UC		550 ± 24
lividomycin A	AcCoA	kanamycin B (25)	UC		115 ± 6
pefloxacin	kanamycin B	AcCoA (50)	C	225 ± 12	
pefloxacin	norfloxacin	AcCoA (500)	C	460 ± 28	
pefloxacin	AcCoA	kanamycin B (100)	UC		126 ± 14
pefloxacin	AcCoA	norfloxacin (400)	UC		8 ± 1

95% D_2O, a region where small changes in pH(D) did not have any effect on kinetic parameters (see below). Reactions were performed at fixed, saturating concentrations of AcCoA and at varying concentrations of the second substrate. The solvent kinetic isotope effects on V were 1.38 ± 0.03 and 1.78 ± 0.05 for kanamycin B and ciprofloxacin, respectively (Figure 2). The solvent kinetic isotope effects on $V/K_{\text{kanamycin B}}$ and $V/K_{\text{ciprofloxacin}}$ were 1.28 ± 0.05 and 1.17 ± 0.04, respectively (Figure 2).

The very low values of the solvent kinetic isotope effects on V/K suggest that both kanamycin and ciprofloxacin are kinetically "sticky" and that no slow, solvent isotopically sensitive step occurs between kanamycin B/ciprofloxacin binding and the first irreversible step, generally assumed to be the release of the first product. The larger values of the solvent kinetic isotope effects on V, which includes steps from the precatalytic ternary complex through final product release, may reflect the effects of solvent isotopic substitution on the chemical step, the release of products, or the conformational changes that allow this to occur. The magnitude of the solvent kinetic isotope effects and inequality of ^{D_2O}V and $^{D_2O}V/K$ argues against a rapid equilibrium mechanism where the chemical step is rate limiting.

pH Profile. AAC(6′)-Ib-wt exhibited an optimum pH of 5.6, while the pH optima for AAC(6′)-Ib-cr were 6.1 and 7.7 for aminoglycoside and fluoroquinolone acetylating activities, respectively. The k_{cat} pH activity profiles of the reactions catalyzed by AAC(6′)-Ib-wt and AAC(6′)-Ib-cr were bell shaped (Figure S2). The k_{cat} pH profile of AAC(6′)-Ib-cr for aminoglycoside acetylation suggests the involvement of two groups exhibiting pK_a values of 5.62 ± 0.06 and 6.84 ± 0.07 whose ionization is critical for catalytic activity. In the case of fluoroquinolone acetylation AAC(6′)-Ib-cr, however, the k_{cat} pH profile reveals that the pK_a values have shifted to 7.08 ± 0.04 and 8.40 ± 0.05. Such a shift of pK_a values in k_{cat} profile could be due to the formation of the enzyme−substrate complex and/or solvent perturbation (*36*). Binding of aminoglycosides to AAC(6′)-Ib-wt is coordinated through several hydrogen-bonding interactions at the active site (see below). The catalytic base Asp115 is involved in two hydrogen-bonding interactions with the aminoglycosides including one with a 6′-NH_2 group where chemistry occurs. Modeling of the potential fluoroquinolone interactions in the active site based on the structural information from AAC(6′)-Ib-wt−AcCoA−aminoglycoside ternary complex (see below) suggests that the fluoroquinolone binding is facilitated by several stacking interactions instead of the numerous hydrogen-bonding interactions that coordinate aminoglycoside binding. This difference in binding interactions between the enzyme and the two substrates may account for the differences in the pK values observed for the catalytic groups.

Overall Fold. The structure of AAC(6′)-Ib-wt in complex with CoA and kanamycin B was recently published (*37*); however, the coordinates were not available at the start of this work. The structure of AAC(6′)-Ib-wt presented here was determined by SAD (single-wavelength anomalous diffraction) utilizing a single mercury derivative collected on a rotating anode source (Table 3). AAC(6′)-Ib is composed of 199 residues and has been determined to be a monomer in solution (*37*). The N-terminal 20 residues are not visible in electron density maps. A construct truncated to Asp21, the first residue visible in AAC(6′)-Ib-wt electron density maps, was as active as full-length AAC(6′)-Ib-wt (data not shown), and Asp21 is 25 Å from the binding site of aminoglycoside on the opposite side of the β-sheet, suggesting the N-terminus is not important for catalysis. The structure is similar to the mixed $\alpha\beta$ fold of other members of the GCN5-related *N*-acetyltransferase (GNAT) family (*38*). The core β-sheet is composed of seven predominately antiparallel β-strands (β4-β5 parallel), with α1 and α2 interacting with one face and α3, α4, and α5 interacting with

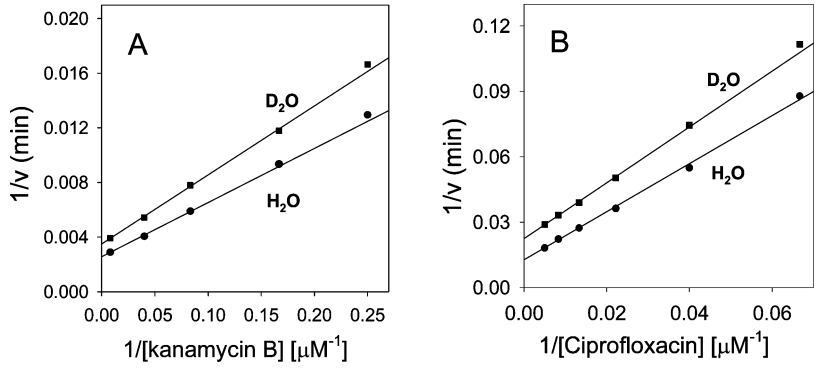

FIGURE 2: Solvent kinetic isotope effect for AAC(6′)-Ib-cr. The symbols are experimentally determined values in H_2O (●) or 95% D_2O (■); the lines are fits of the data to eq 6. Kanamycin B and ciprofloxacin were variable substrates at a fixed, saturating concentration of AcCoA.

Table 3: Crystallographic Data and Refinement Statistics[a,b]

	no soak	RIB/CoA	PAR/AcCoA	HgOAc[c]
Crystal Data				
resolution (Å)	35−2.2 (2.32−2.2)	35−1.7 (1.79−1.7)	35−1.8 (1.9−1.8)	35−2.2 (2.32−2.2)
completeness (%)	99.3 (97.4)	97.0 (84.7)	99.5 (96.6)	100.0 (99.9)
redundancy	15.7 (14.1)	7.4 (6.0)	7.0 (4.0)	13.9 (12.1)
$I/\sigma(I)$	49.4 (18.0)	33.2 (6.9)	34.6 (5.4)	26.5 (6.5)
R_{sym}	0.046 (0.132)	0.040 (0.213)	0.039 (0.215)	0.086 (0.315)
figure of merit[d]				0.29 (0.19)
Model and Refinement Statistics				
resolution (Å)	35−2.2 (2.26−2.2)	35−1.7 (1.74−1.7)	35−1.8 (1.85−1.80)	
no. of reflections	12453	25956	22389	
R_{cryst} (%)	17.7 (18.6)	18.2 (27.4)	18.4 (27.7)	
R_{free} (%)	22.5 (21.2)	21.1 (34.3)	21.6 (32.3)	
no. of atoms, total	1644	1776	1708	
no. of residues	176	179	177	
no. of waters	158	250	204	
average *B*-factor (Å^2)				
protein	17.6	15.4	16.8	
AcCoA (CoA)/ aminoglycoside	37.5/25.9	30.9/14.2	24.8/18.8	
water	25.2	27.6	27.5	
rmsd				
bond lengths (Å)	0.014	0.013	0.015	
bond angles (deg)	1.50	1.335	1.54	

[a] Statistics in parentheses are for the high resolution bin. [b] No sigma cutoffs were applied to data. [c] Values calculated with merged Friedel mates. [d] As calculated in the program PHENIX.

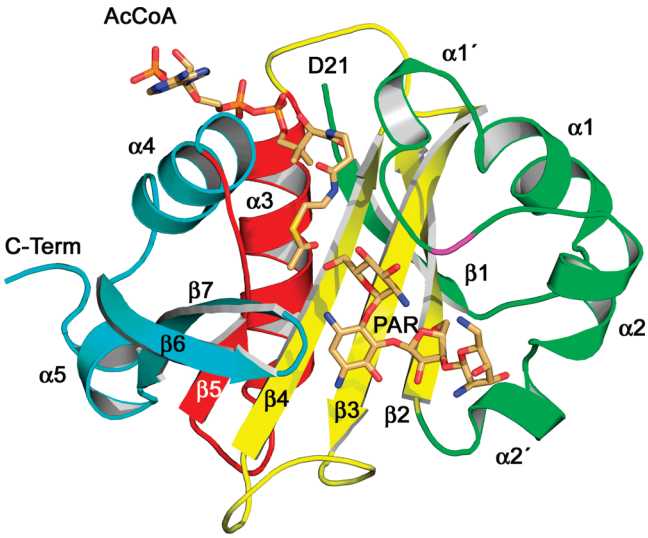

FIGURE 3: Structure of AAC(6′)-Ib-wt. Ribbon diagram of AAC(6′)-Ib-wt in complex with AcCoA and PAR.

the opposite face of the β-sheet (Figure 3). The β-sheet has the order $\beta1$, $\beta2$, $\beta3$, $\beta4$, $\beta5$, $\beta7$, $\beta6$, and there is a disruption of the β-strand interactions between $\beta4$ and $\beta5$ giving the β-sheet a V-like appearance. There does not appear to be any large global structural differences (rmsd of 0.33 Å over 177 common Cα) between the structure of the previously determined AAC(6′)-Ib−CoA−kanamycin B complex (*37*) and the AAC(6′)-Ib−AcCoA−kanamycin C complex determined here.

AcCoA Binding Site. AcCoA binds to AAC(6′)-Ib-wt in a fashion similar to that observed previously with other members of the GNAT superfamily (*38*). The majority of the adenosine 3′,5′-disphosphate moiety is solvent exposed with the 3′-phosphate coordinated by the side chains of Arg162 and Lys166 and the adenine and ribose rings forming nonpolar interactions with α4 (Figure 3, Figure S3A). The 5′-diphosphate (pyrophosphate) interacts substantially with the N-terminal dipole of helix α3 and the $\beta2/\alpha3$ loop, forming five direct and one solvent-mediated hydrogen bond with seven main chain backbone atoms and one side chain atom (Thr130^{OG1}). The pantothenate of AcCoA takes a C-shape as it enters a tunnel formed by the interactions of α1 with α4, with the bend occurring as the pantothenate interacts with the side chain and main chain of Trp48 on α3. The C-shape is also guided by the interactions of the "peptide-like" character of the pantothenate/β-mercaptoethylene moiety with $\beta4$, forming a "β-sheet-like" interaction. The availability of the main chain atoms of $\beta4$ to exogenous ligands is due to the "splaying" of $\beta4$ from $\beta5$ disrupting the β-sheet. While most likely encoded by the entire structure, the maintenance of the $\beta4/\beta5$ disruption in AAC(6′)-Ib-wt may in part be due to two proline residues (Pro153, Pro155), preventing an extension of the $\beta5$ strand. There was clear electron density for the acetyl group of AcCoA with the carbonyl hydrogen bonded to the backbone nitrogen of Gln116 and essentially coplanar with the plane of the central β-sheet (Figure 4).

Aminoglycoside Binding Site. Interestingly, in the AAC(6′)-Ib-wt−AcCoA complex there was additional electron density in the acceptor binding pocket despite the fact that only AcCoA was included in the crystallization conditions (Figure 4A). This electron density was consistent with a 4,6-disubstituted deoxystreptamine ring and could be successfully fit as kanamycin presumably originating from the expression conditions (60 μM kanamycin) and retained during purification on Ni-NTA agarose chromatography. In this complex, the 6′-polar group is approximately 2.2 Å from the *re* face of the thioester, suggesting that if the 6′-substituent were a primary amine, that turnover should have occurred yielding acetylated aminoglycoside and CoA. There are two possible explanations for the observation of both an acceptor and donor molecule occurring in the active site with no turnover. The enzyme may not be active in the solid state, with perhaps the lack of enzyme motion or correctly positioned active site residues preventing turnover, or the acceptor molecule is actually an inhibitor rather than a substrate. The kanamycin used in expression was kanamycin sulfate purified from

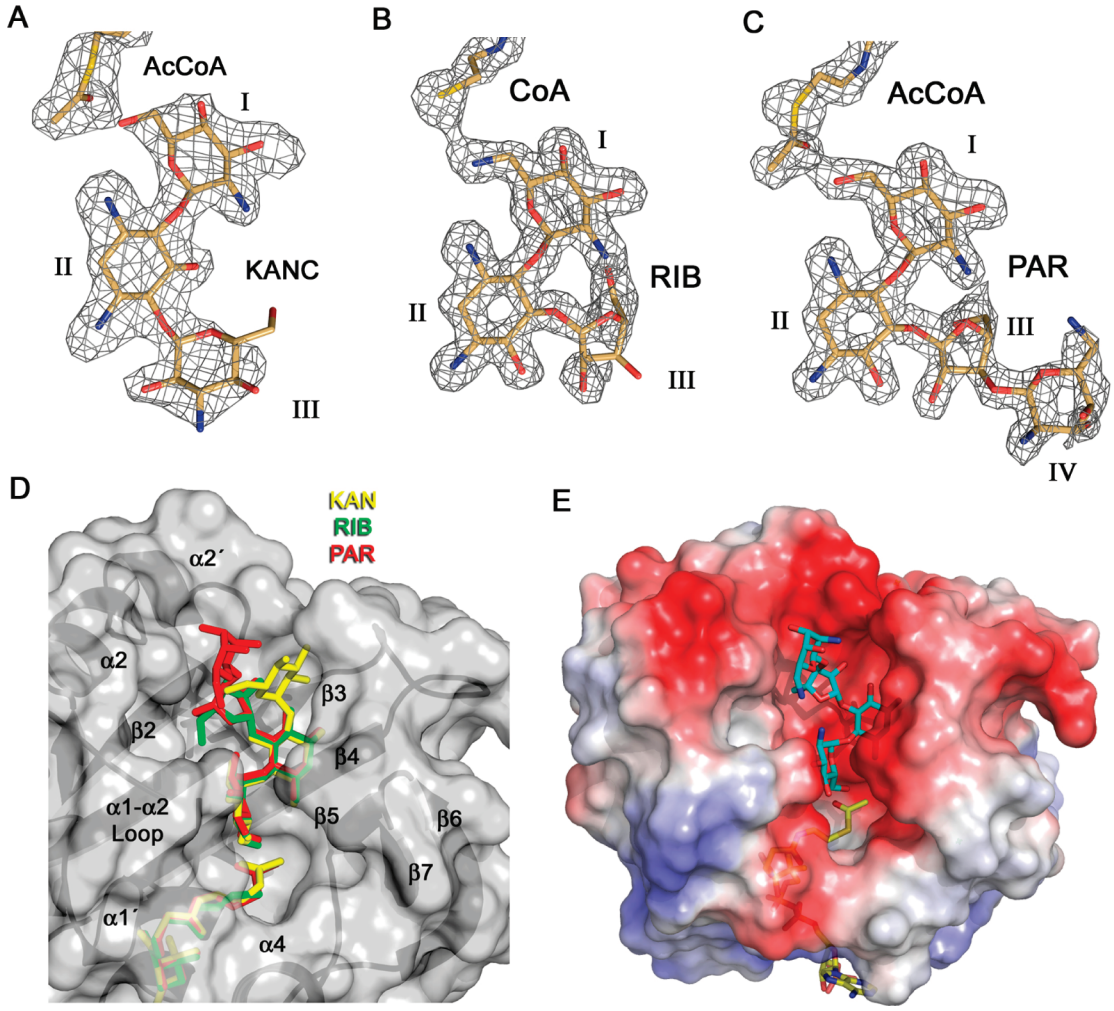

FIGURE 4: $F_o - F_c$ randomized omit map for bound aminoglycoside and donor moiety (S−H or S−$COCH_3$) of CoA contoured at 2.5σ for the (A) KANC/(AcCoA), (B) RIB/(CoA), and (C) PAR/(AcCoA) complexes. Prior to calculation of the electron density map temperature factors were set to 20 Å^2, random errors were added to the coordinates to yield an rmsd of 0.25 Å to the parent structure, the ligands were removed, and the resulting structure was refined for 10 cycles in REFMAC. (D) Superposition of the KANC/AcCoA, RIB/CoA, and PAR/AcCoA complexes with AAC(6′)-Ib. Molecular surface and ribbon diagram of AAC(6′)-Ib are shown in gray and black, respectively. (E) Electrostatic potential of AAC(6′)-Ib mapped on the molecular surface contoured at ±5 kT (red, negative; blue, positive). PAR and AcCoA shown as sticks and colored with blue and yellow carbons, respectively.

Streptomyces kanamyceticus (SIGMA K1377). Commercial kanamycin purified from producing organisms contains predominately kanamycin A but also contains small amounts of kanamycins B and C (*39, 40*). The 6′-polar substituent on kanamycins A and B is an amine while on kanamycin C it is a hydroxyl group. To discern between these two possibilities, an additional two AAC(6′)-Ib-wt complexes were attempted by soaking crystals with the 4,5-disubstituted aminoglycosides ribostamycin (RIB) and paromomycin (PAR). 4,5-Disubstituted aminoglycosides were chosen because they would provide clear evidence for displacement of the bound 4,6-disubstituted aminoglycoside. In the case of the AAC(6′)-Ib-wt−RIB and −PAR complexes, the data clearly demonstrate an exchange of the 4,5-disubstituted aminoglycoside which followed along during purification with the 4,6-disubstituted aminoglycoside which was used to soak the crystals. In the case of the ribostamycin complex where the 6′-polar group is a primary amine, the data show clear electron density for CoA and unacetylated ribostamycin (Figure 4B). This is the expected result if the AAC(6′)-Ib-wt crystals were catalytically competent, and ribostamycin was in great excess to AcCoA (RIB 5 mM, AcCoA none added in soak). In contrast, the 6′-polar group of paromomycin is a hydroxyl, and the data show clear electron density for AcCoA and unacetylated paromomycin with rings I−III in a similar conformation as seen in the AAC(6′)-Ib-wt−ribostamycin complex (Figure 4C). The AAC(6′)-Ib-wt−PAR complex demonstrates that AAC(6′)-Ib-wt can bind aminoglycosides with 6′-OH groups in a catalytically favorable conformation but does not possess the catalytic active site groups to promote the more difficult acetylation of a hydroxyl group. The ribostamycin and paromomycin complexes suggest that the aminoglycoside which remained bound during purification was kanamycin C, originating from the expression media, and as such this presumption was used in the final rounds of refinement of that data set. The binding of kanamycin C to AAC(6′)-Ib is essentially identical to that observed in the published structure of AAC(6′)-Ib to CoA and kanamycin B (*37*).

The aminoglycoside binding site is constructed as a box with β-strands 2, 3, and 4 as the base and the β3-β4 loop with α1′, α2, α2′, β6, β7 and their intervening loops as the walls (Figure 3). Aminoglycoside rings I and II are bound by narrow constrictions of the active site, while rings III and

IV interact with a more open surface depression. In the kanamycin C complex, rings I and III bind perpendicular to the β-sheet, while ring II is parallel (Figure 4D). In the paromomycin and ribostamycin complex rings II and III are parallel to the β-sheet, while rings I and IV are perpendicular. There are no large-scale structural rearrangements or conformational changes between the three complex structures. The AAC(6′)-Ib-wt−RIB and AAC(6′)-Ib-wt−PAR structures exhibit rmsds of 0.35 and 0.33 Å with the AAC(6′)-Ib-wt−KAN complex over 175 common Cαs. The largest deviations occur away from catalytically important residues and involve interactions with rings III and IV. The $\beta3/\beta4$ loop takes a different conformation in the kanamycin C complex versus the 4,5-disubstituted aminoglycoside complexes. In the kanamycin C complex, ring III is directed at the $\beta3/\beta4$ loop, and there is a peptide flip of residues Leu96 and Ser98 that permits optimization of the interaction between the backbone carbonyl of Ser98 with the 3″-NH_3 and the side chain of Asp100 with the 3″-NH_3 and 4″-OH. In the ribostamycin and paromomycin complexes, the aminoglycoside is directed away from the $\beta3/\beta4$ loop and Asp100 points in the opposite direction toward solvent. There are minor shifts in the positioning of the $\alpha2'/\beta2$ loop, which appears directed by the interaction of Glu73 with rings III and IV. The side chain of Glu73 takes different conformations in all three complexes, making 0, 1, and 3 interactions with the ribostamycin, kanamycin C, and paromomycin complexes, respectively. Finally, there is weak electron density for residues 51−54 ($\alpha1'$-$\alpha2$ loop) that was only sufficient in the AAC(6′)-Ib-wt−RIB complex to build a model. Ribostamycin, however, makes no direct contacts with residues from this loop, and therefore its ordering is most likely due to longer order solvation effects. The interactions with the rings get fewer in number and appear to be less specific from ring II to ring IV. Ring II is the most buried ring and has the lowest average *B*-factors (PAR, 12.5 $Å^2$), followed by ring I (PAR, 17.5 $Å^2$), then ring III and IV (PAR, 25.1 and 34.1 $Å^2$). There are a total of eight acidic side chains, which are scattered throughout the acceptor binding cavity and no compensating basic side chains, making the active site very negatively charged, ideal for attracting and interacting with positively charged aminoglycosides (Figure 4E, Figures S3B and S4A,B). The structure suggests that Asp115 and Asp152 are the most critical acidic residues in the active site, with Asp115 and Asp152 forming buried ionic interactions with the 6′-NH_2 and 3-NH_2 of aminoglycoside rings I and II and Asp115 positioned to act as a proton acceptor during catalysis (see below). Three tryptophan residues make significant contributions to the active site. The side chains of Trp49 ($\alpha1'$-$\alpha2$ loop) and Trp102 ($\beta3$-$\beta4$ loop) make stacking interactions with rings I and II, respectively, and the side chain of Trp103 makes a direct hydrogen bond with the 1-NH_3 of ring II (Figure 5A). The stacking interactions are optimized by rings I and II being in the chair conformation with the amino and hydroxyl substituents in the equatorial positions giving the rings a flat structure. On the opposite face of the ring II-Trp102 stacking is a second stacking arrangement with Tyr93, which is enhanced by the interaction of the 1-NH_2 with the aromatic π system.

The structure therefore suggests that the acceptor binding site has a high-affinity binding site for the structural feature which is identical in all commonly used aminoglycosides, a central 2-deoxystreptamine ring (ring II), and an arrangement of aromatic side chains whose planar surfaces are ideal for interacting with the chair conformation of rings I and II and their 1,4 linkage. In addition, the narrow and more specific binding site for rings I and II opens into a more expansive and flexible surface groove with several potential polar handles, a structure that is consistent with the ability of AAC(6′)-Ib-wt to bind and acetylate a wide variety of aminoglycosides with 6′-NH_2 groups.

Enzyme Mechanism. AAC(6′)-Ib-wt could catalyze the transfer of the acetyl group directly to the 6′-NH_2 or indirectly through a covalent enzyme-acyl intermediate. AAC(6′)-Ib-wt has a single cysteine, Cys163, located in the middle of $\alpha3$, with its side chain pointing toward the AcCoA binding site. Its thiol group, however, is over 11 Å from the acceptor binding site and is unlikely to participate in catalysis. A Cys163Ala mutant resulted in expressing cells that retained resistance to amikacin and kanamycin (*41*). The structure of the AAC(6′)-Ib-wt ternary complexes with AcCoA and aminoglycosides with a 6′-OH substituent clearly support a direct transfer mechanism (Figures 4 and 5). In these complexes the 6′-OH polar group is 2.2 (KANC) and 2.7 Å (PAR) from the *re* face of the acetyl group and in ideal geometry for direct transfer. In addition, these structures suggest that Asp115, which is directly interacting with the 6′-group, could act as a general base to accept a proton during the reaction mechanism. *E. coli* carrying a plasmid encoded AAC(6′)-Ib-wt with the corresponding aspartate mutated to an alanine lost the aminoglycoside resistance phenotype (*42*). The backbone amide of Asn116 is hydrogen bonded to the carbonyl group of AcCoA, and its partial positive charge could assist in polarization of the carbonyl group to stabilize the tetrahedral intermediate. A semiconserved tyrosine among GNAT enzymes, Tyr164, located on $\alpha3$ could potentially act as an active site acid to protonate the sulfhydryl of CoA. There is great debate, however, on the role of this particular residue, and it is not always conserved among GNATs. For example, the mutation of the related tyrosine to a phenylalanine in serotonin acetyltransferase led to a 290-fold reduction in k_{cat} (*43*). Studies of the mutation of the same residue in AAC(6′)-Ii to an alanine were found not to be consistent with this tyrosine acting as a general acid (*44*). In contrast to the observations with the serotonin acetyltransferase structures, Tyr164 is not hydrogen bonded to the thiolate of CoA. In AAC(6′)-Ib-wt the side chain of Tyr164 is pulled toward $\beta4$ and away from the sulfhydryl (~4.1 Å OH−S) by the interaction of the phenolic hydroxyl of Tyr164 with the side chain of Gln116 and is actually much closer to the carbonyl oxygen of AcCoA (~3.0 Å). One possibility is that the deformation of the acetyl group toward tetrahedral geometry during the reaction disrupts the Tyr164−Gln116 interaction or displaces the sulfhydryl of CoA down toward Tyr164 such that Tyr164 can act as a general acid. A second distinct possibility is that a number of water molecules (6−8) directly adjacent to the 6′-NH_3 could function to shuttle a proton from bulk solvent to protonate the sulfhydryl of CoA in a pocket bordered by $\alpha3$ and $\beta7$. The bell-shaped pH curve suggests that the protonation states of two protein groups are important for catalysis, with the most likely candidates being Asp115 and Tyr164.

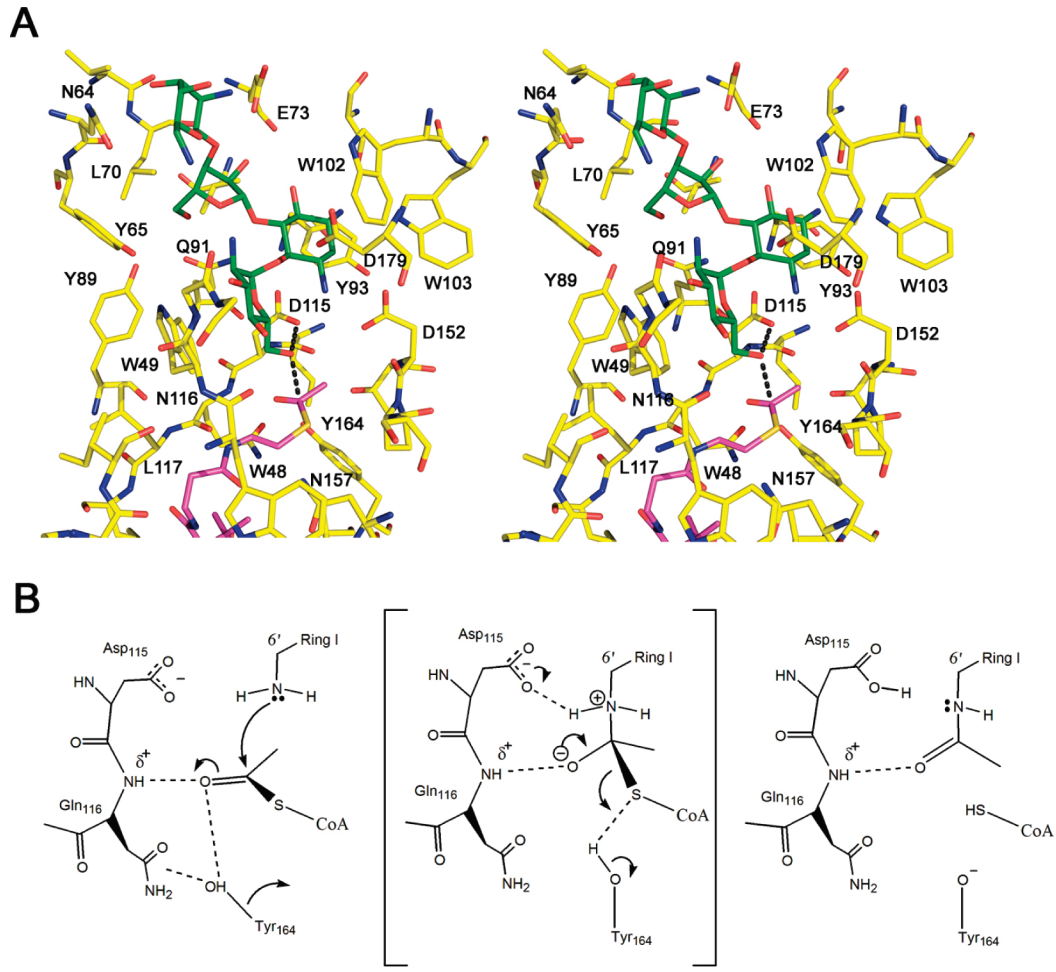

FIGURE 5: Proposed mechanism of AAC(6′)-Ib-wt. (A) Stereo diagram of residues within 5 Å of aminoglycoside and AcCoA in the AAC(6′)-Ib-wt−PAR−AcCoA complex. Protein residues are shown with yellow carbons and PAR and AcCoA with green and magenta carbons, respectively. Interactions of the 6′-OH with Asp115 and the acetyl carbon of AcCoA are shown as dotted black lines. (B) Schematic of the AAC(6′)-Ib-wt enzyme mechanism with direct attack of the aminoglycoside amine on the *re* face of the acetyl group of AcCoA and formation of a tetrahedral intermediate.

Trp102Arg/Asp179Tyr Mutation. Attempts to crystallize the AAC(6′)-Ib-cr double mutant were unsuccessful; however, the structural determination of the AAC(6′)-Ib-wt ternary complexes permits modeling of the potential effects of the mutations on the binding site for fluoroquinolones. Asp179 is located on the $\beta6/\beta7$ loop, and its side chain interacts with aminoglycoside at one or two points through water molecules. Trp102 is located on the $\beta3/\beta4$ loop, and its side chain forms stacking interactions with ring II of bound aminoglycosides and has packing interactions with the side chains of Pro178 and Asp179 of the $\beta6/\beta7$ loop. The molecular model was created with several restrictions implied by the data. Since the mutant protein retained significant activity against aminoglycosides, the altered side chains should enhance the binding of fluoroquinolones while not interfering with binding of aminoglycosides. The fluoroquinolone should be positioned such that the amino nitrogen of its piperazinyl substituent should be in a position to attack the *re* face of the AcCoA acetyl group yet still allow access of Asp115 to act as the general base. The geometry of attack and the planarity of fluoroquinolones necessitate that the plane of the fluoroquinolone be nearly perpendicular to the *re* face of AcCoA; therefore, the fluoroquinolone cannot interact with many of the structural features utilized in coordinating aminoglycosides, the glycosidic linkages of which permit significant deviations from perpendicularity to the *re* face in rings II, II, and IV. In the final AAC(6′)-Ib-cr ciprofloxacin model, the amino nitrogen of its piperazinyl moiety is 2.7 Å from Asp115 and the *re* face of the AcCoA acetyl group. The faces of the fluoroquinolone make stacking interactions with the $\beta6/\beta7$ and $\alpha1'$-$\alpha2$ loops, the cyclopropyl moiety faces out into solvent, and the fluoro, carbonyl, and carboxylate moieties face the aminoglycoside binding pocket (Figure 6). On the $\alpha1'$-$\alpha2$ loop, Trp49 makes interactions with the piperazinyl substituent and/or with the fluorobenzyl portion of the quinolone ring similar to those of Trp49 with ring I of aminoglycoside. Gly50−Ala54 are a region of high flexibility such that Gly50 and Gly51 can form productive van der Waal interactions with the face of the pyridinone ring of the quinolone. On the $\beta6/\beta7$ loop, the side chain of Asp179 is unlikely to provide positive interactions with the quinolone ring. A tyrosine at this position, in the same rotomer position, would provide a significantly better interaction due to π-stacking of the p-orbitals of the tyrosine and quinolone rings. Asp179 is located adjacent to the surface such that the Asp179Tyr side chain could adopt several different rotomers, and residue 49 is most likely critical to stabilizing the proper rotomer of residue 179. In the case of the Trp102Arg mutation the guanidinium group of the arginine can make a perpendicular

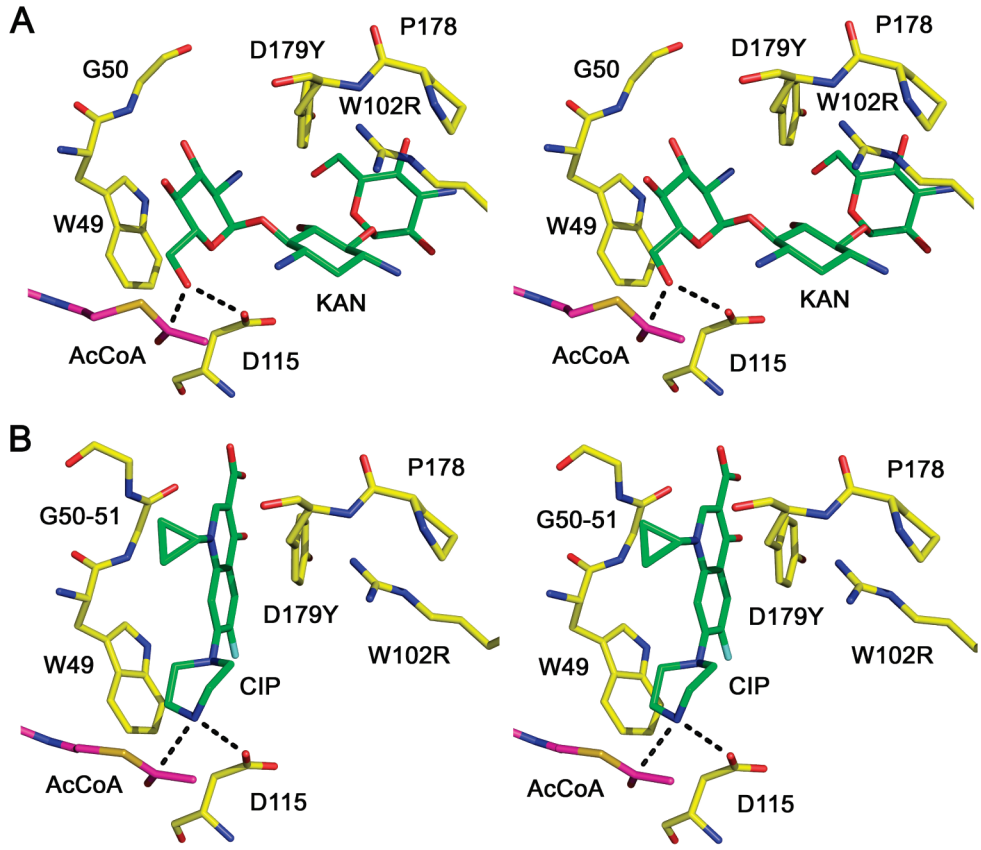

FIGURE 6: Stereo diagram illustrating the model of the interaction of (A) KANC and (B) CIP with the Asp179Tyr/Trp102Arg−AAC(6′)-Ib-cr mutant, illustrating the interaction of the acceptor with the acetyl group of AcCoA and Asp115.

π-cation interaction with the tyrosine face opposite the quinolone holding it in a productive rotomer. The conformations of the side chains in the mutations would not adversely affect the binding of aminoglycosides, as the side chain of Tyr179 fills a void adjacent to the aminoglycoside, and Arg102 occupies the same space as the Trp and can replicate the stacking interactions with the ring II of aminoglycoside. The model therefore suggests that the Asp179Tyr mutation is responsible for the increase in the affinity of AAC(6′)-Ib-cr for fluoroquinolones and that the Trp102Arg mutation stabilizes the correct rotomer of the tyrosine while maintaining the productive interactions between the $\beta6/\beta7$ and $\beta3/\beta4$ loops. This model is further supported by the fact that the Asp179Tyr mutant alone conferred a 2-fold rise in the MIC of ciprofloxacin and the two mutations together (Asp179Tyr and Trp102Arg) conferred a 3−4-fold rise (*22*). Maurice et al. (*37*) report an alternate hypothesis for the binding of fluoroquinolones to AAC(6′)-Ib-cr which utilized molecular dynamics and a bound HEPES molecule as a starting point. In their model they propose a similar interaction of the Asp179Tyr mutation with the fluoroquinolone, although they propose the fluoroquinolone binds in same position as aminoglycosides and with the Trp102Arg mutation interacting with the fluoroquinolone carboxylate. The model presented here requires less structural rearrangement and places the secondary amine of the fluoroquinolone in more conducive geometry to form a ternary complex with clear access to Asp115, the active site base. However, we cannot rule out that the structural plasticity of AAC(6′)-Ib demonstrated in the Maurice paper could facilitate their proposed binding mode for fluoroquinolones and suggest both models are equally valid.

The mechanism elucidated here further highlights the adaptive potential of AACs that in this case is presumably driven by the selective pressures of fluoroquinolone use. Surveys of clinical isolates of enteric bacteria from around the world have reported the cr allele of *aac(6′)-Ib* that in several studies now constitutes a quarter or more of all alleles of *aac(6′)-Ib* (*22*, *52*, *53*). That alleles encoding only single mutations of Asp179Tyr or Trp102Arg have not been reported also supports the importance of the enzyme stabilizing role of Trp102Arg in allowing Asp179Tyr to promote ciprofloxacin positioning and catalysis, as elucidated in the structural model.

SUPPORTING INFORMATION AVAILABLE

Schematic depicting structures of the aminoglycosides and fluoroquinolones used in the study, graphs of the pH activity profiles, and detailed Chemdraw depictions of the interactions of AAC(6′)-Ib with CoA and aminoglycosides. This material is available free of charge via the Internet at http://pubs.acs.org.

REFERENCES

1. Magnet, S., and Blanchard, J. S. (2005) Molecular insights into aminoglycoside action and resistance. *Chem. Rev. 105*, 477–498.
2. Miller, G. H., Sabatelli, F. J., Naples, L., Hare, R. S., and Shaw, K. J. (1995) The changing nature of aminoglycoside resistance mechanisms and the role of isepamicin—a new broad-spectrum aminoglycoside. The Aminoglycoside Resistance Study Groups. *J. Chemother. 7* (Suppl. 2), 31–44.

3. Wright, G. D. (1999) Aminoglycoside-modifying enzymes. *Curr. Opin. Microbiol. 2*, 499–503.
4. Davies, J., and Wright, G. D. (1997) Bacterial resistance to aminoglycoside antibiotics. *Trends Microbiol. 5*, 234–240.
5. Poole, K. (2005) Efflux-mediated antimicrobial resistance. *J. Antimicrob. Chemother. 56*, 20–51.
6. Hooper, D. C. (2001) Mechanisms of action of antimicrobials: focus on fluoroquinolones. *Clin. Infect. Dis. 32* (Suppl. 1), S9–S15.
7. Ruiz, J. (2003) Mechanisms of resistance to quinolones: target alterations, decreased accumulation and DNA gyrase protection. *J. Antimicrob. Chemother. 51*, 1109–1117.
8. Hooper, D. C. (1999) Mechanisms of fluoroquinolone resistance. *Drug Resist. Updates 2*, 38–55.
9. Li, X. Z. (2005) Quinolone resistance in bacteria: emphasis on plasmid-mediated mechanisms. *Int. J. Antimicrob. Agents 25*, 453–463.
10. Robicsek, A., Jacoby, G. A., and Hooper, D. C. (2006) The worldwide emergence of plasmid-mediated quinolone resistance. *Lancet Infect. Dis. 6*, 629–640.
11. Jacoby, G. A. (2005) Mechanisms of resistance to quinolones. *Clin. Infect. Dis. 41* (Suppl. 2), S120–S126.
12. Wang, M., Sahm, D. F., Jacoby, G. A., and Hooper, D. C. (2004) Emerging plasmid-mediated quinolone resistance associated with the qnr gene in *Klebsiella pneumoniae* clinical isolates in the United States. *Antimicrob. Agents Chemother. 48*, 1295–1299.
13. Vakulenko, S. B., and Mobashery, S. (2003) Versatility of aminoglycosides and prospects for their future. *Clin. Microbiol. Rev. 16*, 430–450.
14. Rather, P. N., Munayyer, H., Mann, P. A., Hare, R. S., Miller, G. H., and Shaw, K. J. (1992) Genetic analysis of bacterial acetyltransferases: identification of amino acids determining the specificities of the aminoglycoside 6′-N-acetyltransferase Ib and IIa proteins. *J. Bacteriol. 174*, 3196–3203.
15. Kim, C., Villegas-Estrada, A., Hesek, D., and Mobashery, S. (2007) Mechanistic characterization of the bifunctional aminoglycoside-modifying enzyme AAC(3)-Ib/AAC(6′)-Ib′ from *Pseudomonas aeruginosa*. *Biochemistry 46*, 5270–5282.
16. Azucena, E., Grapsas, I., and Mobashery, S. (1997) Properties of a bifunctional antibiotic resistance enzyme that catalyzes ATP-dependent 2″-phosphorylation and acetyl-CoA-dependent 6′-acetylation of aminoglycosides. *J. Am. Chem. Soc. 119*, 2317–2318.
17. Daigle, D. M., Hughes, D. W., and Wright, G. D. (1999) Prodigious substrate specificity of AAC(6′)-APH(2″), an aminoglycoside antibiotic resistance determinant in enterococci and staphylococci. *Chem. Biol. 6*, 99–110.
18. Boehr, D. D., Jenkins, S. I., and Wright, G. D. (2003) The molecular basis of the expansive substrate specificity of the antibiotic resistance enzyme aminoglycoside acetyltransferase-6′-aminoglycoside phosphotransferase-2. The role of ASP-99 as an active site base important for acetyl transfer. *J. Biol. Chem. 278*, 12873–12880.
19. Kim, C., Hesek, D., Zajicek, J., Vakulenko, S. B., and Mobashery, S. (2006) Characterization of the bifunctional aminoglycoside-modifying enzyme ANT(3″)-Ii/AAC(6′)-IId from *Serratia marcescens*. *Biochemistry 45*, 8368–8377.
20. Dubois, V., Poirel, L., Marie, C., Arpin, C., Nordmann, P., and Quentin, C. (2002) Molecular characterization of a novel class 1 integron containing bla(GES-1) and a fused product of aac3-Ib/aac6′-Ib′ gene cassettes in *Pseudomonas aeruginosa*. *Antimicrob. Agents Chemother. 46*, 638–645.
21. Tolmasky, M. E., Roberts, M., Woloj, M., and Crosa, J. H. (1986) Molecular cloning of amikacin resistance determinants from a *Klebsiella pneumoniae* plasmid. *Antimicrob. Agents Chemother. 30*, 315–320.
22. Robicsek, A., Strahilevitz, J., Jacoby, G. A., Macielag, M., Abbanat, D., Park, C. H., Bush, K., and Hooper, D. C. (2006) Fluoroquinolone-modifying enzyme: a new adaptation of a common aminoglycoside acetyltransferase. *Nat. Med. 12*, 83–88.
23. Leslie, A. G. (2006) The integration of macromolecular diffraction data. *Acta Crystallogr., Sect. D: Biol. Crystallogr. 62*, 48–57.
24. Evans, P. (2006) Scaling and assessment of data quality. *Acta. Crystallogr., Sect. D: Biol. Crystallogr. 62*, 72–82.
25. Adams, P. D., Gopal, K., Grosse-Kunstleve, R. W., Hung, L. W., Ioerger, T. R., McCoy, A. J., Moriarty, N. W., Pai, R. K., Read, R. J., Romo, T. D., Sacchettini, J. C., Sauter, N. K., Storoni, L. C., and Terwilliger, T. C. (2004) Recent developments in the PHENIX software for automated crystallographic structure determination. *J. Synchrotron Radiat. 11*, 53–55.
26. Perrakis, A. (1997) wARP: Improvement and Extension of Crystallographic Phases by Weighted Averaging of Multiple-Refined Dummy Atomic Models. *Acta Crystallogr. D53*, 448–455.
27. Emsley, P., and Cowtan, K. (2004) Coot: model-building tools for molecular graphics. *Acta Crystallogr., Sect. D: Biol. Crystallogr. 60*, 2126–2132.
28. Murshudov, G. N., Vagin, A. A., and Dodson, E. J. (1997) Refinement of macromolecular structures by the maximum-likelihood method. *Acta Crystallogr., Sect. D: Biol. Crystallogr. 53*, 240–255.
29. Schuttelkopf, A. W., and van Aalten, D. M. (2004) PRODRG: a tool for high-throughput crystallography of protein-ligand complexes. *Acta Crystallogr., Sect. D: Biol. Crystallogr. 60*, 1355–1363.
30. Martel, A., Masson, M., Moreau, N., and Le Goffic, F. (1983) Kinetic studies of aminoglycoside acetyltransferase and phosphotransferase from *Staphylococcus aureus* RPAL. Relationship between the two activities. *Eur. J. Biochem. 133*, 515–521.
31. Williams, J. W., and Northrop, D. B. (1978) Kinetic mechanisms of gentamicin acetyltransferase I: Antibiotic-dependent shift from rapid to nonrapid equilibrium random mechanisms. *J. Biol. Chem. 253*, 5902–5907.
32. Magalhaes, M. L., and Blanchard, J. S. (2005) The kinetic mechanism of AAC3-IV aminoglycoside acetyltransferase from *Escherichia coli*. *Biochemistry 44*, 16275–16283.
33. Hegde, S. S., Javid-Majd, F., and Blanchard, J. S. (2001) Overexpression and mechanistic analysis of chromosomally encoded aminoglycoside 2′-N-acetyltransferase (AAC(2′)-Ic) from *Mycobacterium tuberculosis*. *J. Biol. Chem. 276*, 45876–45881.
34. Magnet, S., Lambert, T., Courvalin, P., and Blanchard, J. S. (2001) Kinetic and mutagenic characterization of the chromosomally encoded *Salmonella enterica* AAC(6′)-Iy aminoglycoside N-acetyltransferase. *Biochemistry 40*, 3700–3709.
35. Draker, K. A., Northrop, D. B., and Wright, G. D. (2003) Kinetic mechanism of the GCN5-related chromosomal aminoglycoside acetyltransferase AAC(6′)-Ii from *Enterococcus faecium*: evidence of dimer subunit cooperativity. *Biochemistry 42*, 6565–6574.
36. Cleland, W. W. (1982) The use of pH studies to determine chemical mechanisms of enzyme-catalyzed reactions. *Methods Enzymol. 87*, 390–405.
37. Maurice, F., Broutin, I., Podglajen, I., Benas, P., Collatz, E., and Dardel, F. (2008) Enzyme structural plasticity and the emergence of broad-spectrum antibiotic resistance. *EMBO Rep. 9*, 344–349.
38. Vetting, M. W., de Carvalho, L. P. S., Yu, M., Hegde, S. S., Magnet, S., Roderick, S. L., and Blanchard, J. S. (2005) Structure and functions of the GNAT superfamily of acetyltransferases. *Arch. Biochem. Biophys. 433*, 212–226.
39. Maeda, K., Ueda, M., Yagishita, K., Kawaji, S., Kondo, S., Murase, M., Takeuchi, T., Okami, Y., and Umezawa, H. (1957) Studies on kanamycin. *J. Antibiot. (Tokyo) 10*, 228–231.
40. Rothrock, J. W., Goegelman, R. T., and Wolf, F. J. (1958) A resin chromatographic analysis for kanamycin mixtures. *Antibiot. Annu. 6*, 796–803.
41. Shmara, A., Weinsetel, N., Dery, K. J., Chavideh, R., and Tolmasky, M. E. (2001) Systematic analysis of a conserved region of the aminoglycoside 6′-N-acetyltransferase type Ib. *Antimicrob. Agents Chemother. 45*, 3287–3292.
42. Pourreza, A., Witherspoon, M., Fox, J., Newmark, J., Bui, D., and Tolmasky, M. E. (2005) Mutagenesis analysis of a conserved region involved in acetyl coenzyme A binding in the aminoglycoside 6′-N-acetyltransferase type Ib encoded by plasmid pJHCMW1. *Antimicrob. Agents Chemother. 49*, 2979–2982.
43. Scheibner, K. A., De Angelis, J., Burley, S. K., and Cole, P. A. (2002) Investigation of the roles of catalytic residues in serotonin N-acetyltransferase. *J. Biol. Chem. 277*, 18118–18126.
44. Draker, K. A., and Wright, G. D. (2004) Molecular mechanism of the enterococcal aminoglycoside 6′-N-acetyltransferase′: role of GNAT-conserved residues in the chemistry of antibiotic inactivation. *Biochemistry 43*, 446–454.

BI800664X